

Investigating the effects of ultra-rapid, rapid vs. final precise orbit and clock products on high-rate GNSS-PPP for capturing dynamic displacements

Cemal O. Yigit^{*1,2}, Ahmed El-Mowafy¹, Mert Bezcioglu² and Ahmet A. Dindar³

¹School of Earth and Planetary Sciences, Curtin University, GPO Box U 1987, Perth, WA, Australia

²Department of Geomatics Engineering, Gebze Technical University, 41400, Gebze, Turkey

³Department of Civil Engineering, Gebze Technical University, 41400, Gebze, Turkey

(Received May 9, 2019, Revised August 26, 2019, Accepted October 15, 2019)

Abstract. The use of final IGS precise orbit and clock products for high-rate GNSS-PPP proved its effectiveness in capturing dynamic displacement of engineering structures caused by earthquakes. However, the main drawback of using the final products is that they are available after approximately two weeks of data collection, which is not suitable for timely measures after an event. In this study, the use of ultra-rapid products (observed part), which are available after a few hours of data collection, and rapid products, which are available in less than 24 hrs, are investigated and their results are compared to the more precise final products. The tests are designed such that harmonic oscillations with different frequencies and amplitudes and ground motion of a simulated real earthquake are generated using a single axis shake table and the PPP was used to capture these movements by monitoring time-change of the table positions. To evaluate the accuracy of PPP using ultra-rapid, rapid and final products, their results were compared with relative GNSS positioning and LVDT (Linear Variable Differential Transformer) data, treated as reference. The results show that the high-rate GNSS-PPP solutions based on the three products can capture frequencies of harmonic oscillations and dynamic displacement with good accuracy. There were slight differences between ultra-rapid, rapid and final products, where some of the tested events indicated that the latter two produced are more accurate and provide better results compared to the ultra-rapid product for monitoring short-term dynamic displacements.

Keywords: PPP; high-rate GNSS; structural health monitoring; seismo-geodesy; shake table; precise satellite products

1. Introduction

The improvement of Global Navigation Satellite Systems (GNSS) data processing and the availability of data of high sampling rate, 10 Hz or higher, make GNSS an indispensable and powerful sensor for monitoring dynamic displacements of engineering structures, such as tall building and long-span suspension bridges that are exposed to winds, traffic loads, earthquakes and ground wave motions caused by large earthquakes. The relative GNSS positioning method, which requires simultaneous data collection with at least two GNSS receivers, have been widely used for structural monitoring studies (Çelebi 2000, Erdoğan *et al.* 2007, Yigit *et al.* 2010, Moschas and Stiros 2011, Pehlivan and Bayata 2016, Pehlivan 2018). However, in case of large (mega) earthquakes, the condition of the reference point in relative positioning might be compromised and the relative GNSS positioning method will fail to capture the absolute displacement movements caused by the earthquake (Shu *et al.* 2017). The limitation of relative positioning can be overcome by the use of precise point positioning (PPP) technique, which can provide absolute 3D position using a single GNSS receiver without the need for a reference receiver (Zumberge *et al.* 1997, Kouba and Heroux 2001). To facilitate single point

positioning, the PPP requires external precise satellite orbit and clock corrections (products), and it applies a number of corrections, such as satellite antenna phase center, phase wind-up, solid earth tides. Additionally, the conventional float-ambiguity PPP method takes a long time to reach a converged solution. After convergence, the post-mission PPP method can offer near accuracy to the relative positioning method (Grinter and Janssen 2012).

Previous studies show that high-rate GNSS PPP has been demonstrated to be a powerful and efficient method for earth-crustal deformation (Calais *et al.* 2006, Tiryakioglu *et al.* 2017), deformation monitoring (Martin *et al.* 2015, Yigit *et al.* 2016, Psimoulis *et al.* 2015), GPS seismology (Avallone *et al.* 2011, Xu *et al.* 2013, Nie *et al.* 2016, Paziewski *et al.* 2018, Xu *et al.* 2019), earthquake early warning systems (Li *et al.* 2013) and structural health monitoring (Moschas *et al.* 2014, Yigit 2016, Yigit and Gurlek 2017, Tang *et al.* 2017, Kaloop *et al.* 2018, Gatti 2018). Moreover, seismic waves produced by large earthquakes can be detected by GPS PPP at 1 Hz frequency (Kouba 2003, Xu *et al.* 2013). Their results demonstrated that high-frequency PPP could capture seismic waves with an accuracy of 2-4 mm in horizontal component and sub-cm level in the vertical component. The performance of the post-processed kinematic-PPP method for capturing dynamic movements in the horizontal and vertical directions was also analyzed based on experimenting on flexible model bars (Moschas *et al.* 2014, Yigit 2016, Yigit and Gurlek 2017, Kaloop *et al.* 2018). In these studies, the

*Corresponding author, Professor
E-mail: cyigit@gtu.edu.tr

PPP-derived displacement time series and the derived fundamental natural frequency of the bars were compared with the results obtained using relative GNSS. Most recently, the high-rate GPS PPP method has been applied to real bridge monitoring, and its performance was also compared with the relative GNSS results (Tang *et al.* 2017).

Both real-time service (RTS) and post-mission GNSS-PPP have been tested for structural health-, earthquake-, tsunami-, landslide-monitoring in the last a few years. While the real-time mode is suitable for natural hazard early warning systems, it has a major drawback, where in the event of a quake, the infrastructure (e.g. Internet) that broadcast RTS might not be available. Post-mission mode, on the other hand, does not need real-time reception of the corrections, and it is used in assessing the detailed health condition of structures and in understanding the behaviour and mechanism of ground motions after the natural events (e.g. earthquake). The assessment of the health condition of any engineering structures after a natural event is vital and necessary for preventing future disasters and saving lives. For this reason, post-mission GNSS-PPP is also required to obtain precise and accurate displacement history since its accuracy is typically better than real-time GNSS-PPP.

In the past studies, the International GNSS Service (IGS) final orbit and clock corrections (products) were used in post-mission processing as they have the highest quality among all available product types. However, this product is available 13-17 days after the last observation. Thus, it is not suitable for a timely response, where assessment should be carried out as soon as possible in order to determine the danger level in the structure and make a decision on the actions that need to be taken. However, along with the final products, there are the ultra-rapid (observed part) and rapid products, the former in available after a few hours and the later in less than 24 hrs. Therefore, in this study, the use of ultra-rapid (observed) and rapid products, are investigated and their results are compared to the more precise final products. The evaluation will focus on the ability of PPP using these products in capturing dynamic displacements for structural monitoring and seismo-geodetic applications. The study, therefore, will show to practitioners the performance differences of using the different available post-mission PPP products in this unique field. A shake table with the ability to move in the horizontal plane and in a single direction was used to generate harmonic motions and to simulate a real earthquake. The GNSS data collected at 10 Hz rate. The PPP results using the three products (final, rapid, and ultra-rapid) are compared to reference data from relative GNSS Positioning and Linear Variable Differential Transformer (LVDT) results to assess their accuracy.

2. PPP mathematical model

The conventional ambiguity-float PPP solution usually uses ionosphere-free (IF) observation combinations along with corrections to the broadcast clock corrections, and precise orbits in post-mission, or orbit corrections to broadcast orbits in real-time processing. The observation equations for code pseudorange and carrier phase

measurements for satellite s in length units can be expressed as (El-Mowafy *et al.* 2016):

$$P_{\mathbf{F}}^s + c \widetilde{dt}^s = \rho^s + c \widetilde{dt}_r + T^s + \varepsilon_{P_{\mathbf{F}}^s} \quad (1)$$

$$\phi_{\mathbf{F}}^s + c \widetilde{dt}^s = \rho^s + c \widetilde{dt}_r + T^s + \lambda_{\mathbf{F}} \widetilde{N}_{\mathbf{F}}^s + \varepsilon_{\phi_{\mathbf{F}}^s} \quad (2)$$

and the biased (real-numbered-float) ambiguity term ($\lambda_{\mathbf{F}} \widetilde{N}_{\mathbf{F}}^s$) is expressed as:

$$\begin{aligned} \lambda_{\mathbf{F}} \widetilde{N}_{\mathbf{F}}^s = & [(A \lambda_1 N_1^s - B \lambda_2 N_2^s) + (A \delta_{r,1}^s - B \delta_{r,2}^s) \\ & + (A d_1^s - B d_2^s) \\ & - (A d_{r,1} - B d_{r,2})] \end{aligned} \quad (3)$$

where $P_{\mathbf{F}}^s$ and $\phi_{\mathbf{F}}^s$ are the ionosphere-free code and carrier-phase observations, respectively; ρ^s is the satellite-to-receiver geometric range; c is the speed of light in vacuum. It is assumed here that the IGS products for L1 and L2 GPS observations are used and similarly are Natural Resources of Canada (NRCAN) products, such that the biased ionosphere-free combination satellite clock offset $c \widetilde{dt}^s$ includes the satellite code biases (d_1^s and d_2^s), such that $c \widetilde{dt}^s = c dt^s + (A d_1^s - B d_2^s)$, where $c dt^s$ is the original satellite clock offset, $A = \frac{f_1^2}{f_1^2 - f_2^2}$ and $B = \frac{f_2^2}{f_1^2 - f_2^2}$, where f_1 is the L1 carrier frequency (1575.42 MHz), and f_2 is the L2 carrier frequency (1227.6 MHz). Similarly, the biased ionosphere-free combination receiver clock offset $c \widetilde{dt}_r$ includes the receiver code biases ($d_{r,1}$ and $d_{r,2}$), such that $c \widetilde{dt}_r = c dt_r + (A d_{r,1} - B d_{r,2})$, where $c dt_r$ is the unknown receiver clock offset; $\delta_{r,1}^s$ and $\delta_{r,2}^s$ are the combined satellite and receiver phase biases. It is assumed that the receiver hardware biases are the same for measurements of the same frequency for all satellites from the same constellation. Typically, phase delays like phase windup, antenna offset, relativistic errors are estimated from empirical models and are reduced from the phase observations before being used. Finally, $\varepsilon_{P_{\mathbf{F}}^s}$ and $\varepsilon_{\phi_{\mathbf{F}}^s}$ are the ionosphere-free code and carrier-phase observation noise.

In this model, the float ambiguity term ($\lambda_{\mathbf{F}} \widetilde{N}_{\mathbf{F}}^s$) is considered as part of the unknowns that are determined every epoch in the kinematic mode. To avoid rank-defect of the model, code observations are needed. Because of the high noise of code observations and the slow variation of the satellite geometry, the ambiguity values need approximately 30 minutes or more (depending on the observed satellite number and geometry) to stabilize and to converge the solution to the decimeter level of accuracy.

3. NRCAN ultra-rapid & rapid and the IGS final products

In this study, GNSS data was processed using the Canadian Spatial Reference System (CSRS)-PPP software since it is capable of processing both GPS and GLONASS observation with a data rate of 1 Hz or higher. The CSRS-PPP uses the best products available at the time the data is

submitted. This online free software currently uses both NRCAN and IGS products. NRCAN products are also computed using data from the IGS global tracking network. If the GNSS observations are submitted within a few hours after data collection, CSRS-PPP uses the NRCAN ultra-rapid (observed part) product. If data are submitted between the next day and less than 13 days, CSRS-PPP will mainly depend on NRCAN rapid products, and if submitted 13 -17 days later, CSRS-PPP will use the IGS final products (El-Mowafy 2011).

The most frequently updated IGS products are the ultra-rapid products, which are generated four times a day with a latency of three hours. The clock accuracies for the observed part of ultra-rapid that is used in this study is 0.15 ns, whereas the clock accuracy of the rapid product is 0.075 ns (<http://www.igs.org/products>). The satellite clock interval of ultra-rapid and rapid product is 15 and 5 minutes, respectively. Since PPP accuracy is degraded by the long-term unmodelled corrections, it is better to use a higher-rate satellite clock corrections (Tang *et al.* 2019), such as the 30-s interval satellite clock products, for processing high-rate GPS and GLONASS observations to achieve more accurate results. For this reason, CSRS-PPP software uses ultra-rapid and rapid products generated by NRCAN, which apply clock corrections at an interval of 30 seconds. NRCAN Ultra-rapid (also known as EMU) products are generated 24 times a day with a latency of 90 minutes for GPS and 120 minutes for GPS/GLONASS. For detailed and further information about the NRCAN products generation process, please refer to Mireault *et al.* (2008). In addition, we refer to Cerretto *et al.* (2008) for further information about the comparison of EMU ultra-rapid products with IGS ultra-rapid and IGS rapid products. The accuracy of the IGS final orbits and satellite clocks products are ~ 2.5 cm and 0.075 ns, respectively. Since the satellite and clock products provided by IGS and NRCAN have a lower rate than the submitted high-rate GNSS observations, as the case of our study, orbit and clock corrections have to be interpolated.

4. Design of the experiment

Recall that in this study, the performance of high-rate kinematic GNSS-PPP solutions based on ultra-rapid (observed part) and rapid precise orbit and clock products compared with that of the final products, and their ability to capture dynamic displacements of engineering structures and strong ground motions caused by large earthquakes evaluated. For this purpose, a shake table was used, which can generate sinusoidal harmonic movement with different frequencies and amplitudes and can simulate a real earthquake ground motions. In this study, harmonic oscillations and simulation of a real earthquake experiment have been designed and is described in the following section. The shake table used in the experiments is shown in Fig.1 where it has a flat plate with a total stroke (displacement) of ± 190 mm and the GNSS receiver was fixed on it, to capture its motion. The movement of the shake table was provided by an electric motor connected to its plate. The stability of the table, supported on a metal frame, under high-rate motions was maintained by using

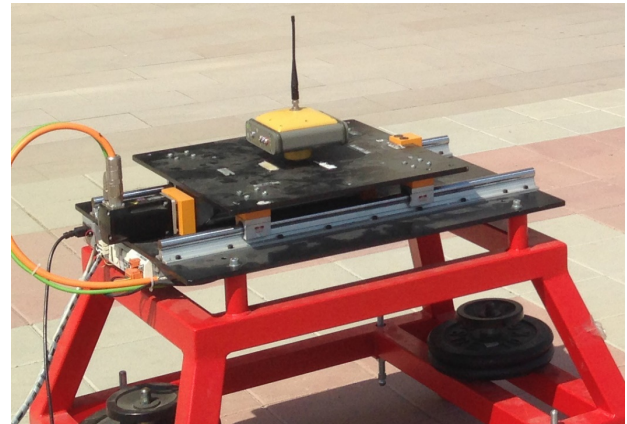


Fig. 1 The Shake Table and GNSS Receiver used in the tests

weights placed on both sides of the platform and anchorage rods of the steel chassis. During the tests, the anchorage rods of the steel chassis were fixed to the ground to prevent lateral movement of the table. The position of the table on the rails was controlled by software running on a Windows computer platform; where the control unit verifies the position using an LVDT embedded under the movable table (not visible in Fig. 1). The LVDT measures the position of the table at a level of mm, with 50 samples per second (50 Hz). The effectiveness of the LVDT and the position of the movable table were regularly checked by external measuring devices.

4.1 Harmonic oscillation and earthquake simulation tests

In order to evaluate the performance of GNSS-PPP method based on different precise orbit and clock products, a large set of harmonic oscillations with different amplitudes and frequencies were generated to cover a wide range of possible structural movements. Twelve experiments with different harmonic oscillations were selected and conducted where the PPP results were compared with a reference LVDT data and relative positioning. Table 1 summarizes these harmonic oscillation events with their frequency and amplitude values. In this study, harmonic oscillations with large amplitude and high frequency were not taken into account since they may cause small deviations to the table that could cause blunders in the results.

Table 1 Oscillation frequency and amplitude of each event selected for this study

		Oscillation Amplitude	
		5 mm	10 mm
Oscillation Frequency	0.2 Hz	Event 1	Event 2
	0.5 Hz	Event 3	Event 4
	1.0 Hz	Event 5	Event 6
	1.5 Hz	Event 7	Event 8
	2.0 Hz	Event 9	Event 10
	2.5 Hz	Event 11	Event 12

In addition to harmonic motions, surface wave motion mimicking those observed during a real earthquake, the El-Centro, was simulated by the shake table. The El-Centro earthquake occurred on May 19, 1940, in Southern California at 05:35 UTC. The earthquake had a moment magnitude (M_w) of 6.9 and was the first major earthquake recorded by strong-motion seismographs. The earthquake was the result of a rupture along the Imperial Fault along with its epicenter, approximately 8.0 km north from Calexico in central California.

4.2 GNSS data collection and data processing

In this study, two dual-frequency Topcon™ HiPer-Pro GNSS receivers were used. GPS and GLONASS observations were collected with a 10° satellite cut-off angle at 10 Hz (0.1 sec.) sampling interval. One GNSS receiver was mounted on the shake table, the other GNSS receiver was installed approximately 20 m away from the shake table at a known station, which served as a reference station for the DD solution in a reference relative positioning mode. The experiment was carried out on 17.08.2016 at the Istanbul Kultur University and lasted approximately 2 hours. The shake table was kept immobile for approximately 30 min from data collection and before starting the harmonic oscillation test to ensure convergence of the ambiguity-float solution for PPP. The rover GNSS data was processed in the reference relative positioning mode using Leica Geo Office (LGO) 3.0 software.

The PPP solution of the rover GNSS data on the shake table was processed in the post-process kinematic PPP mode using CSRS-PPP software. CSRS-PPP software uses the GNSS orbit and clock products (either ultra-rapid, rapid and IGS final) based on the time of data submission and the epoch of the last observation in the dataset (Mireault *et al.* 2008). In order to evaluate the effect of ultra-rapid, rapid and final products on dynamic displacements obtained from GNSS-PPP method, RINEX data was submitted to CSRS-PPP after 2 hours from the test (to allow for the use of ultra-rapid products), and re-submitted after 1 day from the test (such that the rapid products are used) and finally 13 days after carrying out the experiments for use of the final precise products.

Since the Geocentric Cartesian coordinates cannot be directly used in structural health monitoring (SHM) and seismological applications, the Cartesian coordinates obtained from CSRS-PPP and LGO were converted to the local topocentric Cartesian system, assuming using the same scale, as follows:

$$\begin{bmatrix} e_t \\ n_t \\ u_t \end{bmatrix} = \begin{bmatrix} -\sin(\lambda_0) & \cos(\lambda_0) & 0 \\ -\sin(\varphi_0) \cdot \cos(\lambda_0) & -\sin(\varphi_0) \cdot \sin(\lambda_0) & \cos(\varphi_0) \\ \cos(\varphi_0) \cdot \cos(\lambda_0) & \cos(\varphi_0) \cdot \sin(\lambda_0) & \sin(\varphi_0) \end{bmatrix} \begin{bmatrix} X_t - X_0 \\ Y_t - Y_0 \\ Z_t - Z_0 \end{bmatrix} \quad (4)$$

where (X_0, Y_0, Z_0) and (φ_0, λ_0) are the geocentric and

ellipsoidal coordinates of the topocentric origin of the coordinate frames, respectively. (X_t, Y_t, Z_t) are the geocentric Cartesian coordinates at time t and (e_t, n_t, u_t) are the topocentric Cartesian coordinates of the point. The topocentric (e_t, n_t) coordinates are next projected onto the movement direction of the shake table using the following formulas:

$$\begin{aligned} x_t^s &= e_t \cdot \sin(\theta) + n_t \cdot \cos(\theta) \\ y_t^s &= e_t \cdot \cos(\theta) - n_t \cdot \sin(\theta) \end{aligned} \quad (5)$$

where θ refers to the angle of rotation between the coordinate systems (topocentric and shake table). θ is measured and calculated from two adjacent GNSS points along the movement direction of the shake (x_t^s) . x_t^s and y_t^s are the coordinates along and perpendicular to the movement direction, respectively.

5. Results and discussions

In this section, the PPP performance in capturing harmonic movements, using the three different orbit and clock products, is first assessed by comparing their results with LVDT and relative solution in both the frequency and time domains. Next, the PPP solutions when simulating a real earthquake are analyzed.

5.1 Overall displacement performance

To compare the performance of the PPP solutions using the three products (ultra-rapid, rapid and final), the time series of overall displacements obtained from these solutions are plotted versus those obtained from the reference LVDT and relative GNSS positioning. Fig. 2 shows all harmonic oscillation events and earthquake simulation experiment of these solutions. The top panel in the figure (shown in black colour) illustrates displacement obtained from LVDT data with 50 Hz sampling rate, the second panel from top (in magenta colour) represents the displacement derived from the relative GNSS positioning solution using a 10 Hz sampling rate, while the following panels (in blue, red and green colours) represent the tested GNSS-PPP derived displacements (using also a 10 Hz sampling rate) employing the ultra-rapid, rapid and final products, respectively. It is worth noting that this sequence of the sub-plots will be followed in all coming figures. In Fig. 2, the events selected for this study are indicated by red arrows along with the event number as illustrated in the top panel of the figures. It is clear that LVDT and relative positioning derived displacement are very consistent, whereas PPP-derived displacements show a low frequency (long-term) fluctuation. This is mainly due to applying ambiguity float solutions, and other factors such as residual troposphere, multipath propagation error, and the accuracy and precision of the satellite orbit and clock corrections. At first glance from the figure, the three sets of PPP solutions generally produce similar results. However, PPP-ultra-rapid based displacement time series contains sudden shifts, which are marked by ellipses with cyan colour, and PPP consistently continues to capture the dynamic displacement

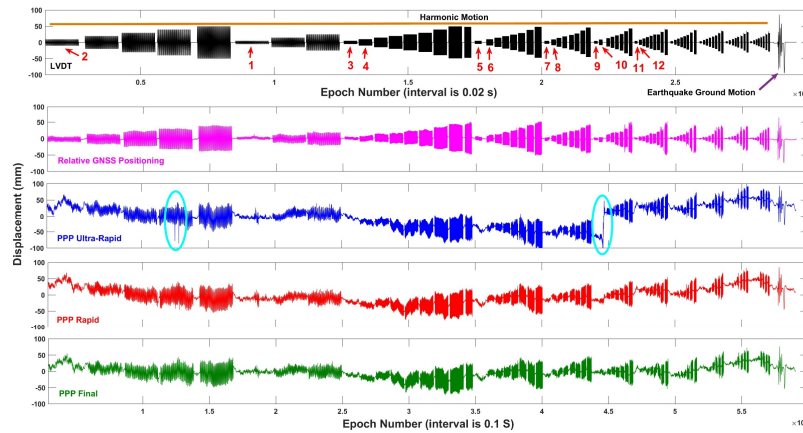


Fig. 2 Overall LVDT (top panel), Relative GNSS positioning (second panel from top), and PPP derived displacement (ultra-rapid, rapid and final, are then given respectively)

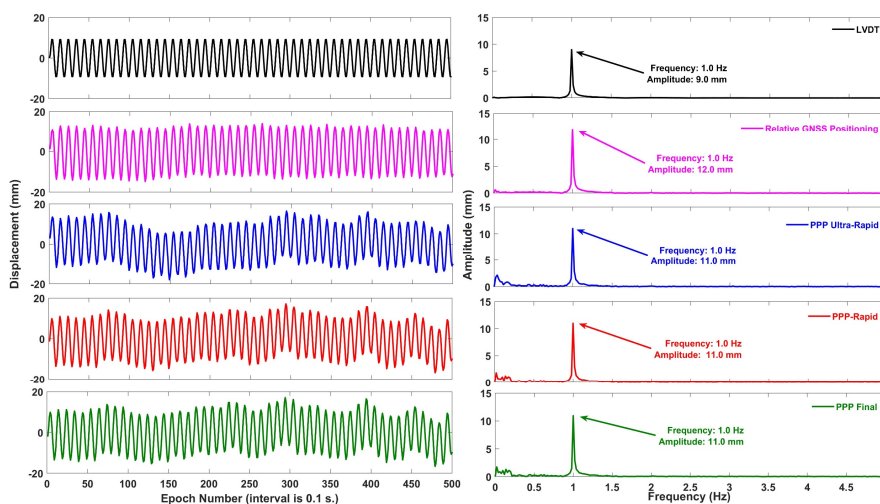


Fig. 3 Displacement time series (left) and FFT spectrum (right) for (from top to bottom): LVDT, relative GNSS positioning, and the three PPP solutions, respectively, for a given 1 Hz frequency with 10 mm of the amplitude of the shake table movement

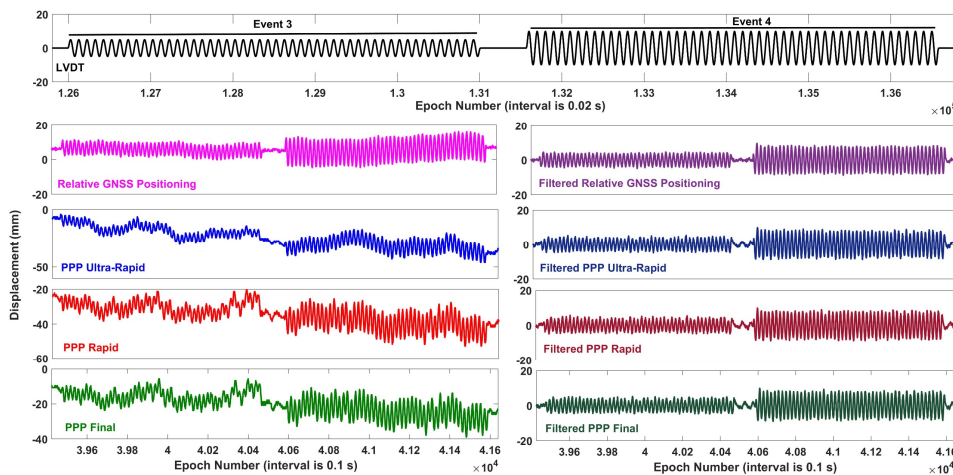


Fig. 4 Displacement time series of LVDT, unfiltered and filtered of relative GNSS positioning and the three PPP solutions using different products for a given 0.5 Hz frequency with 5 mm (left panel) and 10 mm (right panel) of amplitude

after this offset. This offset can also be seen in PPP-rapid derived time series, but with a much smaller value than that of PPP employing ultra-rapid. This offset is attributed to a small jump in the clock corrections. This sudden shift will be investigated and explained in the following section.

5.2 Results of harmonic oscillation tests

To illustrate and compare the performance of the three PPP methods in capturing the harmonic oscillations, three events were chosen as representative examples and results are plotted. As mentioned earlier, the sampling rates of

Table 2 Peak frequency and amplitude for all events using different methods (The amplitude values in square brackets represent the filtered results, whereas the other values indicate unfiltered results.)

Event No (cf. Table 1)	LVDT		Relative GNSS Positioning		PPP ultra-rapid		PPP rapid		PPP final	
	Freq. (Hz)	Amp. (mm)	Freq. (Hz)	Amp. (mm)	Freq. (Hz)	Amp. (mm)	Freq. (Hz)	Amp. (mm)	Freq. (Hz)	Amp. (mm)
1	0.2	5.0	0.2	4.8 [4.6]	0.2	4.5 [4.3]	0.2	4.9 [4.6]	0.2	4.8 [4.6]
2	0.2	9.8	0.2	9.7 [9.4]	0.2	10.3 [9.9]	0.2	10.1 [9.6]	0.2	10.1 [9.6]
3	0.5	4.7	0.5	4.8 [4.8]	0.5	4.9 [4.8]	0.5	5 [4.9]	0.5	5 [4.9]
4	0.5	9.3	0.5	9.7 [9.6]	0.5	9.8 [9.7]	0.5	9.9 [9.9]	0.5	9.9 [9.9]
5	1.0	4.5	1.0	6.1 [6.1]	1.0	5.7 [5.6]	1.0	5.7 [5.6]	1.0	5.7 [5.6]
6	1.0	9.0	1.0	12 [11.8]	1.0	11 [10.8]	1.0	11 [10.9]	1.0	11 [10.8]
7	1.5	4.4	1.5	6.2 [6.1]	1.5	5.8 [5.8]	1.5	5.6 [5.6]	1.5	5.6 [5.6]
8	1.5	8.7	1.5	11.5 [11.4]	1.5	10.7 [10.7]	1.5	10.1 [10.0]	1.5	10.1 [10.0]
9	2.0	4.0	2.0	4.3 [4.2]	2.0	3.7 [3.7]	2.0	3.7 [3.7]	2.0	3.7 [3.7]
10	2.0	8.0	2.0	9.1 [8.9]	2.0	7.2 [7.2]	2.0	7.2 [6.9]	2.0	7.8 [7.7]
11	2.5	4.0	2.5	4.1 [3.9]	2.5	3.6 [3.6]	2.5	3.5 [3.5]	2.5	3.5 [3.5]
12	2.5	7.9	2.5	7.4 [7.1]	2.5	6.6 [6.5]	2.5	6.4 [6.3]	2.5	6.4 [6.3]

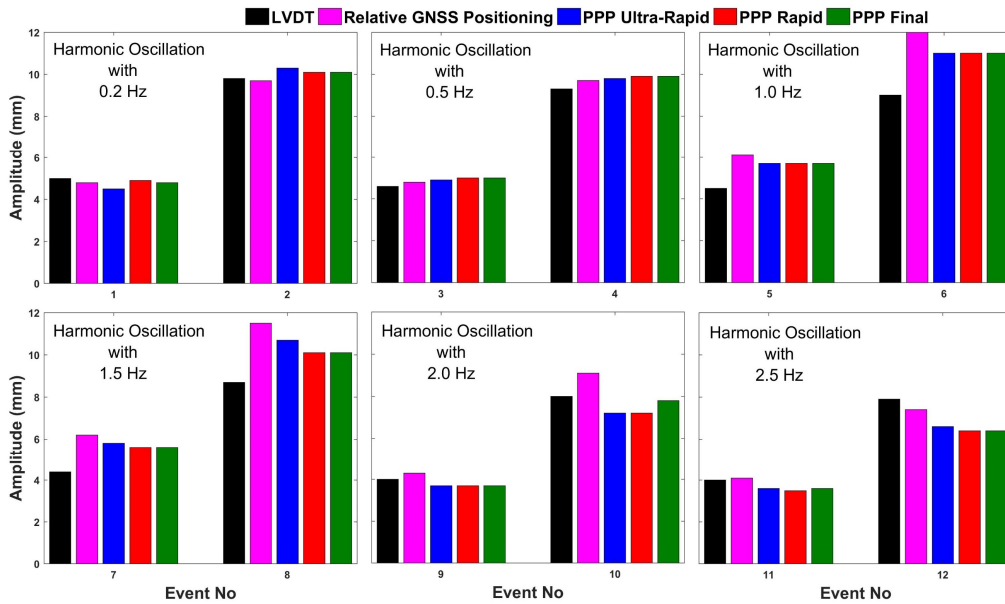


Fig. 5 Peak amplitude for all events using different methods

GNSS and LVDT data are different, which were 10 Hz for the former and 50 Hz for the latter. Therefore, the LVDT data was “down-sampled” to 10 Hz for comparison purpose. Fig. 3 shows displacements in the time domain and FFT (Fast Fourier Transform) spectrums in the frequency domain of the first representative event (characterized by a 1 Hz frequency with 10 mm amplitude). Due to the presence of offsets and a local trend as shown in Fig. 2, each harmonic event obtained from the PPP solutions was first independently de-trended to remove such trend and offsets. From Fig. 3, it can be seen that the displacements estimated by the PPP de-trended solutions show a good agreement with the displacements derived from LVDT and relative GNSS positioning. However, all PPP solutions contain low-frequency components other than the tested 1 Hz frequency within a short period of time (50 seconds for this event). In addition, in the frequency domain, according

to FFT analysis, the oscillation frequencies obtained from all methods are similar, but there are small differences in the amplitudes corresponding to the oscillation frequency.

Differences between the three sets of PPP and the LVDT can be attributed to multipath, and precision of the satellite orbit and clock products. When comparing the three sets of PPP solutions with each other, the amplitude values of peak frequencies obtained are consistent with no significant differences.

The low-frequency components of the three sets of PPP solutions (from using separately the ultra-rapid, rapid and final products) and relative GNSS positioning obtained from harmonic oscillation tests were next filtered out by implementing a fifth-order Butterworth high pass filter with a cut-off frequency of 0.15 Hz. Fig. 4 shows unfiltered and next filtered time series for event numbers 3 and 4 (cf. Table 1). Again the panels of the figures from top to bottom

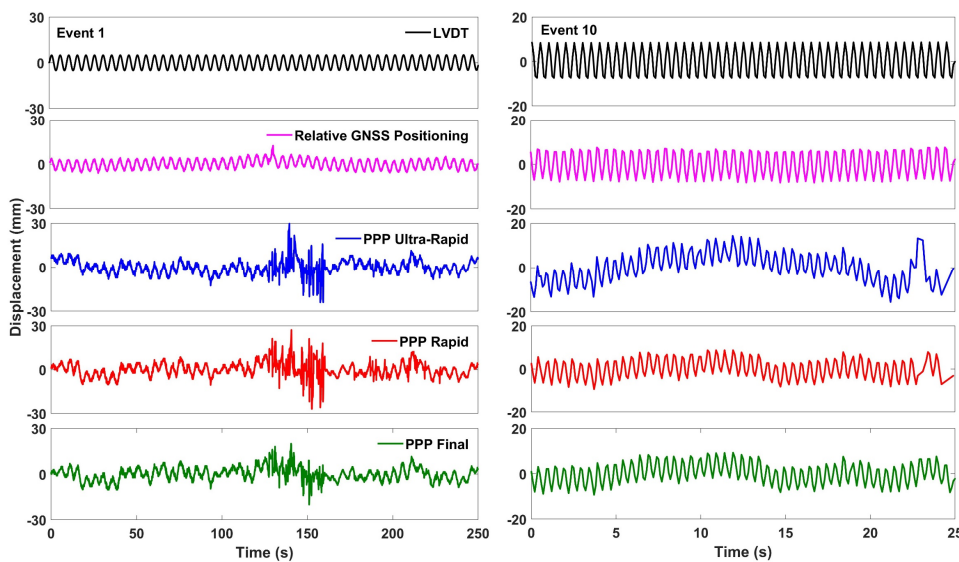


Fig. 6 Time series of the displacement in Event 1 (left) and Event 10 (right) of different solution types

Table 3 Maximum and RMSE values of displacement differences between the three PPP solutions (using ultra-rapid, rapid and final solutions) and LVDT and Relative solution (denoted as Rel.)

Event No (Cf. Table1)	PPP ultra-rapid				PPP rapid				PPP final			
	Max (mm)		RMS (mm)		Max (mm)		RMS (mm)		Max (mm)		RMS (mm)	
	LVDT	Rel.	LVDT	Rel.	LVDT	Rel.	LVDT	Rel.	LVDT	Rel.	LVDT	Rel.
1	32.6	29.6	5.0	5.2	26.0	24.5	5.3	5.2	19.2	23.4	4.6	4.5
2	19.5	18.3	7.6	7.2	19.2	17.1	7.3	6.8	20.3	17.6	7.7	7.2
3	10.8	9.9	3.7	3.5	11.0	11.3	3.6	3.4	10.9	11.1	3.6	3.4
4	7.9	8.1	2.8	2.7	6.7	6.9	2.6	2.4	7.4	6.8	2.7	2.5
5	11.5	10.7	4.5	4.2	13.5	11.8	4.5	4.2	13.2	11.8	4.5	4.2
6	8.8	8.7	3.3	3.0	8.8	7.4	3.1	2.5	8.7	7.5	3.1	2.5
7	6.7	4.7	2.6	1.9	7.1	6.2	2.5	2.1	6.8	6.2	2.5	2.1
8	9.2	8.2	4.0	2.6	8.2	6.5	3.6	2.5	8.5	6.4	3.6	2.5
9	5.6	5.1	2.2	1.6	4.7	3.3	1.9	1.4	4.7	3.3	1.9	1.4
10	16.8	12.8	7.3	5.7	9.8	5.3	5.1	2.4	9.7	6.2	5.0	2.7
11	6.2	6.0	2.1	2.1	7.6	7.4	2.2	2.3	6.9	6.9	2.2	2.2
12	6.8	5.1	2.3	1.7	5.0	3.9	2.2	1.4	5.4	3.9	2.2	1.4

were the results of LVDT, relative GNSS, ultra-rapid, rapid and final products, respectively. The figure shows that the low-frequency fluctuations of both the relative and PPP derived time series seen before disappeared after applying the high-pass filter and the filtered time series were compatible with the LVDT data.

To further examine the performance of the high-rate PPP, the FFT spectrum of the displacement time series for each event listed in Table 1 was obtained. The peak frequency and the corresponding amplitude of each event are summarized in Table 2. The values in square brackets ([]) represent the filtered results, whereas the other values indicate unfiltered results. It is worth noting that the target displacement of the motions was not achieved particularly at higher frequencies due to the erratic nature of the shake table controller. The exact displacement of the table was measured by the internal LVDT that is used as the reference in this study. Fig. 5 displays the bar graph of the amplitude

values of dominant frequency for easier visual comparison for all tested events of harmonic oscillations with different frequencies. As can be seen from the table and the figure, the oscillation frequencies obtained from the three sets of PPP solutions exhibit a good agreement with LVDT and relative positioning. However, there are slight differences in the amplitudes of the peak frequency. The differences in the amplitude of the oscillation frequency between LVDT and PPP solutions range from 0.1 mm to 2.0 mm. The differences in the amplitude of the oscillation frequency between the relative GNSS positioning and the PPP are between 0.0 and 1.9 mm. However, it is seen that the frequencies and amplitudes obtained from the three sets of PPP solutions are very consistent with each other and the differences are in sub-mm. This implies that the natural frequency of engineering structures or dynamic motion can be captured using PPP with the ultra-rapid product.

In addition to the comparison between various methods

in the frequency domain, RMSE and maximum error values of the displacement differences between PPP solutions and the reference LVDT and relative GNSS solution were calculated to further examine and compare the performance of the three sets of PPP solutions, and results are given in Table 3. Since the filtering process can mask a fair comparison between the three PPP solutions, de-trended time series were used to calculate displacement differences. The RMSE and maximum error values demonstrated that the three different products yielded generally similar results, except for the event 1 and event 10. The RMSE and the maximum errors of PPP-rapid and PPP-final solutions are generally similar to each other and they are slightly better than ultra-rapid. There are also some slight differences of RMSE and maximum values obtained from LVDT and relative solutions. This is because of the presence of a different noise level of LVDT and that of relative positioning. Although most of the spatially-correlated errors, such as satellite and receiver orbital and atmospheric errors can be eliminated by double differencing GNSS data, carrier phase multipath in DD solutions remain as unmodeled signal propagation error, which may significantly affect DD-derived time series.

Event 1 and event 10 were investigated more closely and results are illustrated in Fig. 6. It can be seen from the figure that some parts of event 1 and event 10 demonstrate sudden changes in PPP-derived time series. In addition, for event 1, this sudden change exists in relative positioning results. This is attributed to small undetected errors since these sudden changes exist in both relative and the three PPP solutions. However, while the sudden change was very short in relative solution, the PPP solutions seem to be affected a slightly longer. This part represents similar behavior, or pattern, for the three sets of PPP solutions. But, as can be seen from Table 3 and Fig. 6, PPP-final results are better than the other two PPP solutions, and the PPP-rapid gave better results than the PPP-ultra-rapid in terms of the noise level. In other words, the magnitude of unexpected displacement gradually reduced in case of the rapid and final products, respectively. It is worth mentioning that the oscillation frequencies of the event 1 obtained from the three PPP solutions exhibit a good agreement with LVDT and relative positioning.

Similar to event 1, there is a sudden change in displacements associated to event 10 (see the last part of displacement time series of the right plots in Fig. 6), which gives a different character. As can be seen from the table and figure, the PPP-rapid solution is better than PPP-ultra-rapid solution when considering the maximum difference and RMSE values. The unexpected sudden change does not appear in PPP-final result. It is clear that this behavior in the time series is caused by the generation of the ultra-rapid and rapid products since the relative GNSS solution and the PPP-final solution do not include any sudden changes. In addition, ten epochs between the 23rd and 25th seconds were not estimated in PPP-ultra-rapid and PPP-rapid results while corresponding epochs were estimated in the PPP-final and relative results. These two events indicate that PPP solution based on the final product, as expected, provide better results than the rapid and ultra-rapid products, on the

expense of providing the solutions almost two weeks after the event. This implies that if there is such a behavior in the time series, and if precise and reliable evaluation of any engineering structures relies on post-processed GNSS-PPP solutions, and if decision making is also critical and vital, and can wait for 13 days after the event, processing of GNSS data would best use the final products. Nevertheless, the oscillation frequencies of these two events (1 and 10) obtained from PPP-ultra-rapid and PPP-rapid solutions perfectly match those from LVDT, relative positioning, and PPP-final solution. This indicates that PPP-ultra-rapid and PPP-rapid solutions can be used to rapidly assess the preliminary condition of engineering structures.

5.3 Results of the El-Centro earthquake simulation test

In this section, the performance of high-rate kinematic GNSS-PPP method for seismo-geodetic applications is evaluated. Fig. 7 illustrates the time series of displacement obtained from all methods. It can be seen that displacement waveforms derived from the three sets of PPP, compared with relative GNSS positioning and LVDT are substantially consistent in terms of capturing the dynamic wave motion. Moreover, Fig. 8 shows the histogram of the differences between the three sets of PPP solutions and the LVDT (top panel) and with relative GNSS positioning in the bottom panel of the figure. The histograms are given to show the spread and frequency of the differences. It can be seen that the differences in all PPP solutions are within ± 10 mm. When the RMSE values are examined, the superiority of PPP final and PPP rapid solutions are shown to be remarkable. This implies that GNSS-PPP solutions depending on rapid and final products provide slightly better accuracy than that of the ultra-Rapid solution. However, considering the significant latency of the IGS final and NRCAN rapid products compared to the NRCAN ultra-rapid (observed) products, it is clear that PPP-derived displacement based on ultra-rapid product still provide useful and accurate information for quick and preliminary evaluation of wave motion caused by an earthquake.

6. Conclusions

In this study, the effects of ultra-rapid (observed part), rapid and final precise satellite orbit and clock products on high-rate PPP solution were evaluated based on a large set of harmonic motion events and simulating a real earthquake wave motion generated by a shake table for structural health monitoring and seismo-geodetic applications. Their performance was compared to that of LVDT and relative GNSS positioning, treated as the reference for comparison. The three products have their uses, e.g. the final products are needed when one can wait for approximately two weeks after the occurrence of an earthquake to obtain a precise analysis, whereas the ultra-rapid and rapid products are needed when a quick analysis is needed after the event. They are also needed when real-time products (RTS) are not feasible due to unavailability of the Internet, through which the RTS is provided, because of the quake for instances. In general, the displacement waveforms obtained from the five

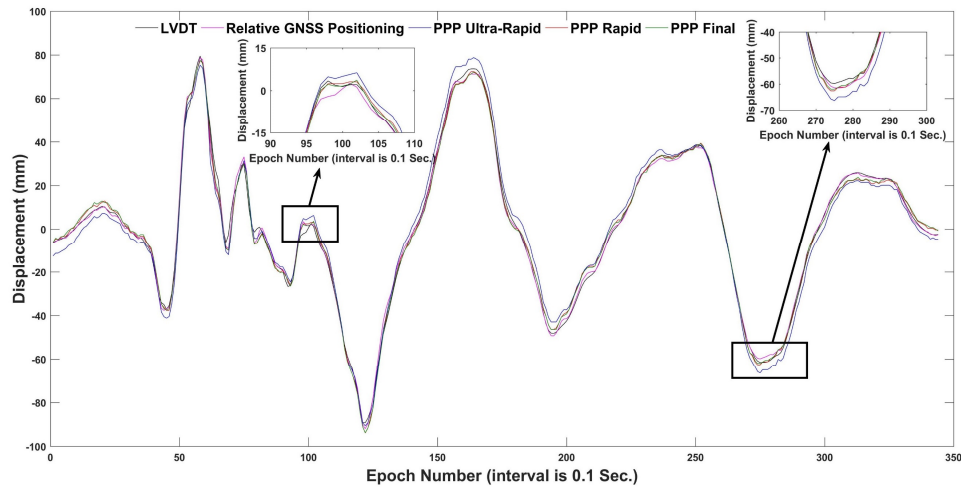


Fig. 7 Comparison of PPP, relative GNSS positioning and LVDT derived displacements at El Centro Earthquake Simulation

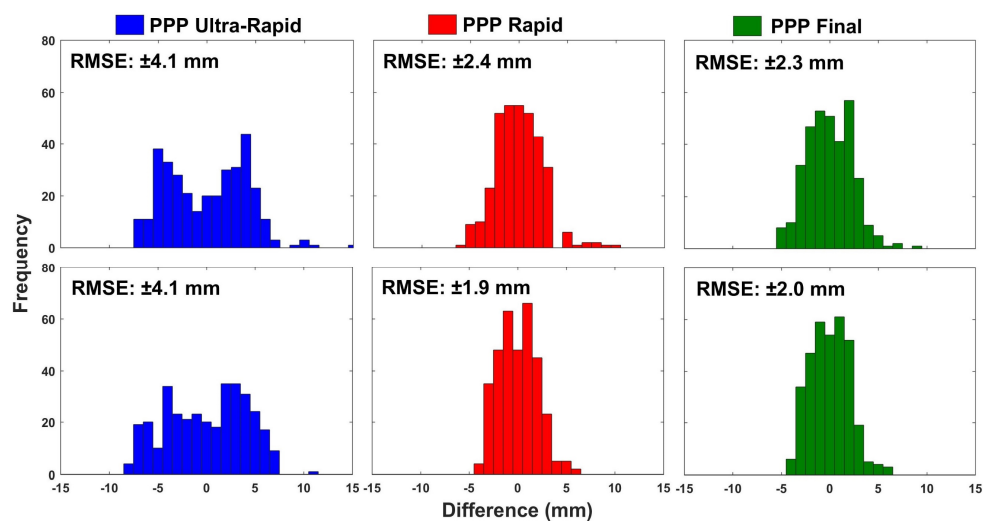


Fig. 8 Histograms of the differences between PPP-derived displacements and LVDT (top panel) and with Relative positioning (bottom panel) for the El Centro earthquake simulation

methods are substantially consistent and the differences between the three PPP solutions and LVDT, or relative GNSS positioning, are sub-centimeters. The results showed that there are no substantial differences between the PPP use when implementing the observed ultra-rapid, rapid and final products, except for event number 1 and event number 10, for the monitoring of short-term dynamic displacements. However, the results of simulating a real earthquake test demonstrated that PPP-derived displacement based on final and rapid products are slightly better than that of the ultra-rapid product. Nevertheless, it is clear that PPP-derived displacement based on the ultra-rapid product still provide useful and accurate information for quick and preliminary evaluation of wave motion caused by an earthquake. Two of twelve events selected from the harmonic experiment demonstrated that PPP-final solution is better than PPP-rapid and PPP-ultra-rapid solutions. However, the displacements when using the PPP-ultra-rapid and PPP-rapid solutions for the two events cover only a small part and the oscillation frequencies obtained from the two solutions perfectly match the LVDT, relative positioning, and PPP-final solution.

Acknowledgments

The first author would like to thank the TUBITAK (Scientific and Technological Research Council of Turkey) Science Fellowships and Grant Programs Department for awarding him a grant to perform a research on High-rate GNSS-PPP Method for GNSS seismology and Structural Health Monitoring Applications including this study at School of Earth and Planetary Sciences, Curtin University, Australia. The authors would also like to thank Natural Resources Canada for providing CSRS-PPP service.

References

- Avallone, A., Marzario, M., Cirella, A., Piatanesi, A., Rovelli, A., Di Alessandro, C., D'Anastasio, E., D'Agostino, N., Giuliani, R. and Mattone, M. (2011), "Very high rate (10 Hz) GPS seismology for moderate-magnitude earthquakes: The case of the Mw 6.3 L'Aquila (central Italy) event", *J. Geophys. Res.*, **116**, B02305. <https://doi.org/10.1029/2010JB007834>.
- Calais, E., Han, J.Y., Demets, C. and Nocquet, J.M. (2006), "Deformation of the North American plate interior from a decade of continuous GPS measurements", *J. Geophys. Res.*, **111**(B6),

- B06402. <https://doi.org/10.1029/2005JB004253>.
- Çelebi, M. (2000), "GPS in dynamic monitoring of long-period structures." *Soil Dyn. Earthq. Eng.*, **20**(5-8, SI), 477-483. [https://doi.org/10.1016/S0267-7261\(00\)00094-4](https://doi.org/10.1016/S0267-7261(00)00094-4).
- El-Mowafy, A. (2011), "Analysis of web-based GNSS post-processing services for static and kinematic positioning using short data spans", *Surv. Rev.*, **43**(323), 535-549. <https://doi.org/10.1179/003962611X13117748892074>.
- El-Mowafy, A., Deo, M. and Rizos, C. (2016), "On Biases in Precise Point Positioning with Multi-Constellation and Multi-Frequency GNSS Data", *Measurement Sci. Technol.*, **27**(3), 035102. <https://doi.org/10.1088/0957-0233/27/3/035102>.
- Erdoğan, H., Akpınar, B., Güllal, E. and Ata, E. (2007), "Monitoring the dynamic behaviors of the Bosphorus Bridge by GPS during Eurasia Marathon", *Nonlinear Proc. Geophys.*, **14**(4), 513-523. <https://doi.org/10.5194/npg-14-513-2007>.
- Cerretto, G., Tavella, P., Lahaye, F., Mireault, Y. and Rovera, D. (2012), "Near real-time comparison and monitoring of time scales with precise point positioning using NRCan ultra-rapid products", *IEEE Transactions on Ultrasonics, Ferroelectrics, and Frequency Control*, **59**(3), 545-551. <https://doi.org/10.1109/TUFFC.2012.2226>.
- Gatti, M. (2018), "Elastic period of vibration calculated experimentally in buildings hosting permanent GPS stations", *Earthq. Eng. Eng. Vib.*, **17**(3), 607-625. <https://doi.org/10.1007/s11803-018-0466-5>.
- Grinter, T. and Janssen, V. (2012), "Post-processed Precise Point Positioning: A viable alternative?", *Proceedings of the 17th Association of Public Authority Surveyors Conference*, Wollongong, NSW, Australia, March, 83-92.
- Kaloop, M.R., Yigit, C.O. and Hu, J.H. (2018), "Analysis of the dynamic behavior of structures using the high-rate GNSS-PPP method combined with a wavelet-neural model: Numerical simulation and experimental tests", *Adv. Space Res.*, **61**(6), 1512-1524. <https://doi.org/10.1016/j.asr.2018.01.005>.
- Kouba, J. (2003), "Measuring seismic waves induced by large earthquakes with GPS", *Stud Geophys Geod.*, **47**(4), 741-755. <https://doi.org/10.1023/A:1026390618355>.
- Kouba, J. and Héroux, P. (2001), "Precise Point Positioning using IGS orbit and clock products", *GPS Solut.*, **5**(2), 12-28. <https://doi.org/10.1007/PL00012883>.
- Li, X., Ge, M., Zhang, X., Zhang, Y., Guo, B., Wang, R., Klotz, J. and Wickert, J. (2013), "Real-time high-rate co-seismic displacement from ambiguity-fixed Precise Point Positioning: application to earthquake early warning", *Geophys Res Lett.*, **40**(2), 295-300. <https://doi.org/10.1002/grl.50138>.
- Martín, A., Anquela, A.B., Dimas-Pagés, A. and Cos-Gayón, F. (2015), "Validation of performance of real-time kinematic PPP. A possible tool for deformation monitoring", *Measurement*, **69**, 95-108. <https://doi.org/10.1016/j.measurement.2015.03.026>.
- Mireault, Y., Tétreault, P., Lahaye, F., Héroux, P. and Kouba, J. (2008), "Online precise point positioning: a new, timely service from natural resources Canada", *GPS World*, September, **19**, 53-64.
- Moschas, F., Avallone, A., Saltogianni, V. and Stiros, S.C. (2014), "Strong motion displacement waveforms using 10-Hz precise point positioning GPS: an assessment based on free oscillation experiments", *Earthq. Eng. Struct. Dyn.*, **43**(12), 1853-1866. <https://doi.org/10.1002/eqe.2426>.
- Moschas, F. and Stiros, S.C. (2011), "Measurement of the dynamic displacements and of the modal frequencies of a short-span pedestrian bridge using GPS and an accelerometer", *Eng. Struct.*, **33**(1), 10-7. <http://dx.doi.org/10.1016/j.engstruct.2010.09.013>.
- Nie, Z., Zhang, R., Liu, G., Jia, Z., Wang, D., Zhou, Y. and Lin, M. (2016), "GNSS seismometer: Seismic phase recognition of real-time high-rate GNSS deformation waves", *J. Appl. Geophys.*, **135**(SI), 328-337. <https://doi.org/10.1016/j.jappgeo.2016.10.026>.
- Paziewski, J., Sieradzki, R. and Baryla, R. (2018), "Multi-GNSS high-rate RTK, PPP and novel direct phase observation processing method: application to precise dynamic displacement detection", *Meas. Sci. Technol.*, **29**(3), 035002. <https://doi.org/10.1088/1361-6501/aa9ec2>.
- Pehlivan, H. and Bayata, H.F. (2016), "Usability of inclinometers as a complementary measurement tool in structural monitoring", *Struct. Eng. Mech.*, **58**(6), 1077-1085. <http://dx.doi.org/10.12989/sem.2016.58.6.1077>.
- Pehlivan, H. (2018), "Frequency analysis of GPS data for structural health monitoring observations", *Struct. Eng. Mech.*, **66**(2), 185-193. <http://dx.doi.org/10.12989/sem.2018.66.2.185>.
- Psimoulis, P., Houlie, N., Meindl, M. and Rothacher, M. (2015), "Consistency of PPP GPS and strong-motion records: case study of Mw9.0 Tohoku-Oki 2011 earthquake", *Sm. Str. Sys.*, **16**(2), 347-366. <http://dx.doi.org/10.12989/sss.2015.16.2.347>.
- Shu, Y., Shi, Y., Xu, P., Niu, X. and Liu, J. (2017), "Error analysis of high-rate GNSS precise point positioning for seismic wave measurement", *Adv. Space Res.*, **59**(11), 2691-2713. <https://doi.org/10.1016/j.asr.2017.02.006>.
- Tang, X., Roberts, G.W., Li, X. and Hancock, C. (2017), "Real-time kinematic PPP GPS for structure monitoring applied on the Severn suspension bridge, UK", *Adv. Space Res.*, **60**(5), 925-937. <https://doi.org/10.1016/j.asr.2017.05.010>.
- Tang, X., Li, X., Roberts, G.W., Hancock, C.M., de Ligt, H. and Guo, F. (2019), "1 Hz GPS satellites clock correction estimations to support highrate dynamic PPP GPS applied on the Severn suspension bridge for deflection detection", *GPS Solut.*, **23**(2), 28. <https://doi.org/10.1007/s10291-018-0813-z>.
- Tiryakioglu, I., Yigit, C.O., Yavasoglu, H., Alkan, R.M. and Saka, M.H. (2017), "The determination of interseismic, coseismic and postseismic deformations caused by the Gokceada-Samothraki earthquake (2014, Mw: 6.9) based on GNSS data", *J. African Earth Sci.*, **133**, 86-94. <https://doi.org/10.1016/j.jafrearsci.2017.05.012>.
- Xu, P., Shi, C., Fang, R., Liu, J., Niu, X., Zhang, Q. and Yanagidani T. (2013), "High-rate precise point positioning (PPP) to measure seismic wave motions: an experimental comparison of GPS PPP with inertial measurement units", *J Geod.*, **87**(4), 361-372. <https://doi.org/10.1007/s00190-012-0606-z>.
- Xu, P., Shu, Y., Niu, X., Yao, W. and Chen, Q. (2019), "High-rate multi-GNSS attitude determination: experiments, comparisons with inertial measurement units and applications of GNSS rotational seismology to the 2011 Tohoku Mw9.0 earthquake", *Meas. Sci. Technol.*, **30**(2), 024003. <https://doi.org/10.1088/1361-6501/aaf987>.
- Yigit, C.O. (2016), "Experimental assessment of post processed kinematic precise point positioning method for structural health monitoring", *Geomat. Nat. Haz. Risk*, **7**(1), 363-380. <https://doi.org/10.1080/19475705.2014.917724>.
- Yigit, C.O., Coskun, M.Z., Yavasoglu, H., Arslan, H. and Kalkan, Y. (2016), "The potential of GPS Precise Point Positioning Method for Point Displacement Monitoring: A Case Study", *Measurement*, **91**, 398-404. <https://doi.org/10.1016/j.measurement.2016.05.074>.
- Yigit, C.O. and Gurlek E. (2017), "Experimental testing of high-rate GNSS precise point positioning (PPP) method for detecting dynamic vertical displacement response of engineering structures", *Geomat. Nat. Haz. Risk*, **8**(2), 893-904. <https://doi.org/10.1080/19475705.2017.1284160>.
- Yigit, C.O., Li, X., Inal, C., Ge, L. and Yetkin, M. (2010), "Preliminary evaluation of precise inclination sensor and GPS for monitoring full-scale dynamic response of a tall reinforced concrete building", *J. Appl. Geod.*, **4**(2), 103-113. <https://doi.org/10.1515/jag.2010.010>.
- Zumberge, J.F., Hefflin, M.B., Jefferson, D.C., Watkins, M.M. and Webb, F.H. (1997), "Precise Point Positioning for the efficient and robust analysis of GPS data from large networks", *J. Geophys. Res.*, **102**(B3), 5005-5017. <https://doi.org/10.1029/96JB03860>.